Dynamics, Simulation & Control of Orbital Modules for On-orbit Assembly

Hrishik Mishra, Tommaso Vicariotto, Marco De Stefano

***Abstract*—In the context of in-orbit assembly, modular building blocks offer the advantage of distributed launches. After the orbit-injection, the overall motion control requires the individual modules to approach each other while regulating their relative shape and the total formation. This kind of formation control has already been addressed for rigid body modules. However, in practical cases, each module might be a multibody (with rotors) system. To address the control problem for such a fleet of fixed-inertia multibody modules, we propose a novel dynamics formulation that is inertia-decoupled, singularity-free, and invariant of their absolute poses. We extend the passive decomposition theory for deriving new representative systems corresponding to the total momentum (locked) and relative shape variations. We exploit the dynamics to design two distinct control laws with complementary mission benefits to regulate the locked and relative motions. We also leverage the proposed formulation to design a Hardware-in-the-Loop (HIL) framework, in which the facility reproduced the relative motions while total momentum was propagated in software. Furthermore, the proposed HIL framework and the motion control are experimentally validated.**

***Index Terms*—Space Robotics and Automation, Multi-Robot Systems, Dynamics, Control.**

I. Introduction

THE economic benefit of distributed launches is driving the assembly of orbital structures towards modular designs which are manufactured on earth and assembled in orbit [1]. To support the in-orbit assembly, the European Union has commissioned the ORU-BOAS project [2], which considers the deployment of orbital modules to perform life-extension operations. These *modules* are autonomous *small* satellites, equipped with on-board Reaction Control System (RCS) and reaction wheels (RWs), i.e., they are fixed-inertia multibody systems. For assembly, two modules are mechanically connected through a dedicated interface, as shown in [2]. After the orbit injection, motion control requires the individual modules to approach each other while regulating their relative shape and the overall (locked) formation. This formation control has already been addressed for rigid body modules using passive decomposition theory [3], [4]. For on-orbit assembly, control strategies have been proposed [5], [6] with rigid body assumptions, and tested on ground [7], [8]. While this assumption was acceptable for large satellites, the couplings with internal actuators (RWs) cannot be neglected in the controller design for small modules with low form factors, see e.g. [2]. In particular, these modules are multibody systems composed of a rigid-body structure with RWs and the related formation control problem has not been addressed before.

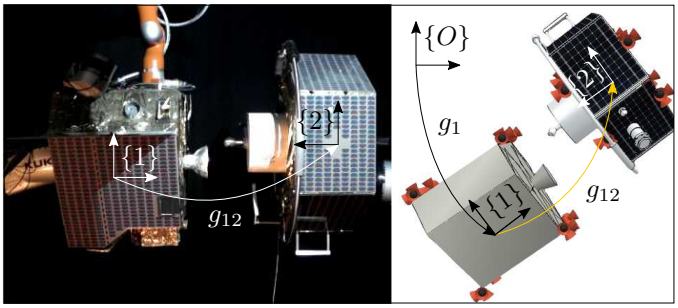

Fig. 1: Formation control between two satellites. Left: The relative motion on the OOS-SIM [9], Right: Absolute motion in software.

During the mission development, the motion control algorithms must undergo on-ground validation, e.g., using relevant 0-g environment replicated by Hardware-in-the-Loop (HIL) robotic simulators [10]. These simulators comprise robotic manipulators, which replicate the 0-gravity motion of an orbital mechanism on-ground. A common approach is to use two industrial robots to replicate the motion of the two orbital agents, see e.g., EPOS [11], INVERITAS [12], Platform-ART [13], AMDS [14] etc. However, the facilities in [11], [12], [13] focus mainly on the approach phases and not contact-phases. In [14], the initial momentum of the satellites is neglected. For validation of mission phases that require contact dynamics, e.g., grasping or docking, an advanced facility with force measurements is employed, e.g., the DLR OOS-SIM (On-orbit Servicing Simulator) [9], shown in Fig. 1. In [15], a Lagrangian matching approach was proposed to achieve full consistency of a single satellite. However, due to limited workspace of the robotic manipulators, this approach becomes limited when absolute motions are large and dynamic. This affects the on-ground demonstration [16]. Therefore, a HIL framework that replicates the relative motion of the agents in a dynamically consistent way is a promising solution [16]. However, in [16], the formulation was considered relative to a nominal trajectory, which required the computation of two dynamic models and also acceleration measurements, which are computational and sensory overheads.

To this end, the contribution of this paper is threefold. First, a momentum-shape dynamics formulation for a fleet of multibody modules is proposed. The contribution here is the sequential application of reduction theory [17] for each

Hrishik Mishra, Tommaso Vicariotto and Marco De Stefano are with the Institute of Robotics and Mechatronics, German Aerospace Center (DLR), 82234 Wessling, Germany. Hrishik Mishra is also with the Automation and Control Institute (ACIN), Technische Universität (TU) Wien, 1040 Vienna, Austria. Tommaso Vicariotto is also with the Department of Mechanical Engineering, Politecnico di Milano, 20156 Milan, Italy. Email: hrishik.mishra@dlr.de, marco.destefano@dlr.de, tommaso.vicariotto@mail.polimi.it)

* Hrishik Mishra and Tommaso Vicariotto contributed equally to this paper.

module followed by passive decomposition theory [3], [4] for the fleet of modules. The key advantage of this formulation is that the motion is described in terms of the total momenta and the shape (relative and RWs motion), which are key mission parameters for motion control. This formulation renders the locked-shape regulation problem time-invariant, unlike simply tracking a leader satellite that requires its acceleration measurements. Second, two complementary control laws: Free-flying and Hierarchical, are proposed to enable on-orbit assembly by regulating the total and relative motions of the modules. The free-flying control law prioritizes convergence, while the hierarchical controller optimizes fuel efficiency. The Cartesian tasks in such missions are time-constrained and necessitate a fast response from the actuators. To achieve this, both control approaches are based on inertia-shaping of RWs' actuator dynamics and passivity-based control of the Cartesian dynamics. Third, a novel HIL simulation framework is realized and experimentally validated on the DLR OOS-SIM, wherein the relative motion is reconstructed on the hardware while simulating momentum in software. The key benefit of this approach is that acceleration measurements are avoided in contrast to [16]. The proposed free-flying controller is experimentally validated using this HIL approach.

The paper is structured as follows. Sec. II introduces the preliminaries which aid the formulation. In Sec. III the proposed method is described. Sec. IV introduces the developed controller. Simulation and hardware results can be found in Sec. V and VI, respectively. Sec. VII concludes the paper.

II. Preliminaries on Dynamics Formulation

In this section, relevant details about rigid body motion on SE(3) group are provided. The pose of a rigid body is a matrix group representation of SE(3) and is written as $g = (R, p)$, where $R \in \mathrm{SO}(3)$ is the rotation matrix and $p \in \mathbb{R}^3$ is the position. The reader is referred to [17], [18] for the detailed descriptions of the introduced quantities. The identity of the SE(3) group is I_4, where I_k is a square identity matrix of dimension k. The tangent space at I_4 is the $\mathfrak{se}(3)$ algebra, which may be referenced in either the body or a spatial frames. Analogously, the cotangent space at I_4 is the dual space of wrenches, denoted as $\mathfrak{se}(3)^*$. The $\mathfrak{se}(3)$ ($\mathfrak{so}(3)$) matrix algebra and its dual $\mathfrak{se}(3)^*$ ($\mathfrak{so}(3)^*$) are isomorphic to the space of body velocities and wrenches on $\mathbb{R}^6$ ($\mathbb{R}^3$). The isomorphisms are written as $(\bullet)^\wedge : \mathbb{R}^3 \to \mathfrak{so}(3), \mathfrak{so}(3)^*$ and $(\bullet)^\vee : \mathfrak{so}(3), \mathfrak{so}(3)^* \to \mathbb{R}^3$, and $(\bullet)^\wedge : \mathbb{R}^6 \to \mathfrak{se}(3), \mathfrak{se}(3)^*$ and $(\bullet)^\vee : \mathfrak{se}(3), \mathfrak{se}(3)^* \to \mathbb{R}^6$, e.g. given a twist, $V \in \mathbb{R}^6$, $V^\wedge \in \mathfrak{se}(3)$. The poses and velocities that are subscripted once are referenced relative to the inertial frame, $\{O\}$, e.g. $(g_1,\ V_1)$ denote the inertial state-space of the leader Satellite's frame, $\mathcal{S}_1$, see Fig. 2. The Adjoint action of a pose g, $\mathrm{Ad} : \mathfrak{se}(3) \to \mathfrak{se}(3)$, transforms elements of $\mathfrak{se}(3)$ algebra between spatial and body frames, see [18]. The adjoint map of the $\mathfrak{se}(3)$ algebra onto itself is, $\mathrm{ad} : \mathfrak{se}(3) \to \mathfrak{se}(3)$, which is the differential of the Ad map. This is denoted by ad_V and its coadjoint map by, $\mathrm{ad}_V^\top : \mathfrak{se}(3)^* \to \mathfrak{se}(3)^*$. In this work, the rigid body velocity follows the convention $V = (v,\, \omega) \cong \mathfrak{se}(3)$, where v (ω) is the linear (angular) velocity, respectively. In this paper, $\mathrm{tr}(\bullet)$ denotes the trace of the argument matrix, and $\mathrm{sk}(\mathcal{X})$ is the skew-part of the argument s.t. $\mathrm{sk}(\mathcal{X}) = \frac{1}{2}(\mathcal{X} - \mathcal{X}^T)$, and $\mathrm{diag}(\bullet)$ is the diagonal concatenation of argument matrices.

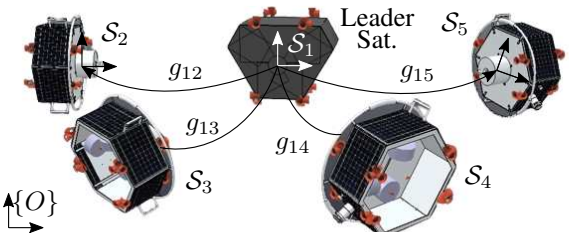

Fig. 2: Fixed-inertia multibody satellites, equipped with RWs and RCS, in a centralized flight formation with $\mathcal{S}_1$ as the leader satellite.

Dynamics of Modules

Each module is modeled as a multibody system comprising its rigid structure and RWs. In a microgravity environment, its dynamics is given by the fixed-inertia Hamel's equations [17]:

$$\mathcal{M}\dot{\zeta} + \mathcal{C}(\zeta)\zeta = F,\ \mathcal{M} = \begin{bmatrix} \begin{bmatrix} m & 0_4 \\ 0_4 & I \end{bmatrix} & \begin{bmatrix} 0_4 \\ I_w A \end{bmatrix} \\ \begin{bmatrix} 0_4 & A^T I_w \end{bmatrix} & A^T I_w A \end{bmatrix} \tag{1}$$
$$\mathcal{C} = \begin{bmatrix} \begin{bmatrix} \omega^\wedge m & 0_4 \\ 0_4 & \omega^\wedge I \end{bmatrix} & \begin{bmatrix} 0_4 \\ \omega^\wedge I_w A \end{bmatrix} \\ 0_{4\times 8} & 0_4 \end{bmatrix}$$

where $\zeta = (v, \omega, \dot{\theta})$, $\dot{\theta} \in \mathbb{R}^3$ is the velocity of the three RWs, and $F = (f_b,\, \tau_b,\, \tau_w)$ comprises the external forces and torques acting on the satellite, and the internal torques, respectively. The inertia matrix is $\mathcal{M}$, while $\mathcal{C}(\zeta)$ is the non-unique centrifugal/Coriolis (CC) matrix. Here, m is the total mass, I and I_w are the locked multibody [17] and RWs inertias, respectively. Also, A is the kinematic map of the RWs frame w.r.t. the module's reference frame. For light-weight modules with three RWs, A is commonly I_3 [19]. Noticeably, Eq.(1) contains couplings among the angular components of the inertia matrix, which requires acceleration measurements to decouple the RWs dynamics from angular motion.

Alternatively, the velocity of a module can be decomposed into a locked angular velocity, computed as a function of the angular momentum, and its shape (RWs) velocity, see [17], [20]. This results in inertia-decoupled dynamics for articulated systems, e.g., a spacecraft equipped with a manipulator. This approach is employed to write the velocities of a module as:

$$\tilde{\zeta} = \begin{bmatrix} v \\ \mu \\ \dot{\theta} \end{bmatrix} = \begin{bmatrix} \xi \\ \dot{\theta} \end{bmatrix} = \begin{bmatrix} I_3 & 0 & 0 \\ 0 & I_3 & \Lambda A \\ 0 & 0 & I_3 \end{bmatrix} \begin{bmatrix} v \\ \omega \\ \dot{\theta} \end{bmatrix} \tag{2}$$

where $\Lambda = (I^{-1} I_w)$ is the dynamic coupling [17]. This term is obtained from the definition of the module's total angular momentum $H_\omega = I\omega + I_w A\dot{\theta}$. Specifically, the new momentum-based velocity term is $\mu = I^{-1} H_\omega$. This velocity decomposition results in inertia-decoupled dynamics as:

$$\tilde{\mathcal{M}}\dot{\tilde{\zeta}} + \tilde{\mathcal{C}}(\tilde{\zeta})\tilde{\zeta} = \tilde{F} \tag{3}$$

where $\tilde{\zeta} = (\upsilon,\, \mu,\, \dot{\theta})$ and $\tilde{F} = (f_b,\, \tau_b,\, \tilde{\tau}_w)$, such that,

$$\tilde{\tau}_w = \tau_w - (\Lambda A)^T \tau_b. \tag{4}$$

The inertia and CC matrices are computed in Appendix 1.

III. Proposed Relative Dynamics

Consider a set of modules, illustrated in Fig. 2, and modeled as in (1). For the sake of simplicity, we derive the dynamics for the scenario comprising two modules, which provides the framework for the n agents problem in Fig. 2. During formation control, the dynamics of two modules is described trivially by stacking (1) for each module as:

$$\tilde{\mathcal{M}}_{1,2}\dot{\tilde{\zeta}}_{1,2} + \tilde{\mathcal{C}}_{1,2}(\tilde{\zeta}_{1,2})\tilde{\zeta}_{1,2} = \tilde{F}_{1,2} \tag{5}$$

where $\tilde{\zeta}_{1,2} = (\xi_1,\, \xi_2,\, \dot{\theta}_1,\, \dot{\theta}_2)$ comprising $\xi_i = (\upsilon_i,\, \mu_i)$ and $\tilde{F}_{1,2} = (f_{b1}, \tau_{b1}, f_{b2}, \tau_{b2}, \tilde{\tau}_{w_1}, \tilde{\tau}_{w_2})$ includes $\tilde{\tau}_{w_i}$, given in (4), and $\tilde{\mathcal{M}}_{1,2} = \text{diag}(M_1, M_2, M_{\theta 1}, M_{\theta 2})$ and $\tilde{\mathcal{C}}_{1,2} = \begin{bmatrix}\tilde{\mathcal{C}}_1^{\xi^\top} & \tilde{\mathcal{C}}_2^{\xi^\top} & \tilde{\mathcal{C}}_1^{\dot{\theta}^\top} & \tilde{\mathcal{C}}_2^{\dot{\theta}^\top}\end{bmatrix}^\top$, s.t. i defines the module's index. See Appendix 1 for the constituent terms in $\tilde{\mathcal{M}}_{1,2}, \tilde{\mathcal{C}}_{1,2}$.

Note that (5) simply stacks the absolute motion of the two modules, while concealing the coupling effects in relative motions. Therefore, we rewrite the dynamics of the two modules by extending the passive decomposition theory, i.e. the motion decomposition into locked and shape systems [3]. The locked system refers to a momentum-based velocity describing the motion of the two modules as a rigid entity, and hence, the total dynamics. On the other hand, the shape system represents the formation within the entity, i.e. the relative dynamics. In contrast with [3] where only rigid bodies were considered, here, we extend the method for fixed-inertia multibody systems, in which the locked-shape dynamics of the formation are coupled with the internal shape (RWs) dynamics of each module, and cannot be ignored in control design.

These representative systems are derived in a centralized fashion. The leader module is designated as $\mathcal{S}_1$, providing a reference for relative quantities, e.g., relative pose g_{12} and velocity ξ_E, computed in the frame attached to $\mathcal{S}_2$. The locked motion is resolved in the frame attached to $\mathcal{S}_1$.

Consequently, the locked and shape velocities, denoted as ξ_L and ξ_E, replace the absolute velocities of the two modules in the novel set of equations of motion. The aforementioned representation is obtained as follows:

$$\xi_L = M_{tot}^{-1} H,\ \xi_E = \xi_2 - \text{Ad}_{g_{12}}^{-1}\xi_1 \tag{6}$$

where M_{tot} is the locked inertia of the two modules, s.t. $M_{tot} = M_1 + \text{Ad}_{g_{12}}^{-T} M_2 \text{Ad}_{g_{12}}^{-1}$, and, H is the total body momentum in the body frame of $\mathcal{S}_1$, computed as,

$$\begin{aligned} H &= M_1\xi_1 + \text{Ad}_{g_{12}}^{-T} M_2(\xi_E + \text{Ad}_{g_{12}}^{-1}\xi_1) \\ &= (M_1 + \text{Ad}_{g_{12}}^{-T} M_2 \text{Ad}_{g_{12}}^{-1})\xi_1 + \text{Ad}_{g_{12}}^{-T} M_2 \xi_E \\ &= M_{tot}\xi_1 + \text{Ad}_{g_{12}}^{-T} M_2 \xi_E. \end{aligned} \tag{7}$$

Therefore, the locked velocity is derived as

$$\begin{aligned} \xi_L = M_{tot}^{-1} H &= \xi_1 + A^*\xi_E,\ A^* = M_{tot}^{-1}\text{Ad}_{g_{12}}^{-T} M_2 \\ &= (I_6 - A^*\text{Ad}_{g_{12}}^{-1})\xi_1 + A^*\xi_2. \end{aligned} \tag{8}$$

As a result, the complete evolution of the initial states, (5), into the new set of representative velocities is accomplished through the following transformation:

$$\underbrace{\begin{bmatrix}\xi_L \\ \xi_E \\ \dot{\theta}_1 \\ \dot{\theta}_2\end{bmatrix}}_{\zeta^*} = \underbrace{\begin{bmatrix} I_6 - A^*\text{Ad}_{g_{12}}^{-1} & A^* & 0 & 0 \\ -\text{Ad}_{g_{12}}^{-1} & I_6 & 0 & 0 \\ 0 & 0 & I_3 & 0 \\ 0 & 0 & 0 & I_3 \end{bmatrix}}_{S} \begin{bmatrix}\xi_1 \\ \xi_2 \\ \dot{\theta}_1 \\ \dot{\theta}_2\end{bmatrix}. \tag{9}$$

We employ this invertible transformation, S, to derive a novel formulation for the dynamics of two modules, encapsulating the total and relative motions in a single set of equations. The new dynamic terms are computed through:

$$\begin{cases} \mathcal{M}^*(g_{12}) = S^{-T}\tilde{\mathcal{M}}_{1,2}S^{-1} \\ \mathcal{C}^*(g_{12}, \zeta^*) = S^{-T}\tilde{\mathcal{C}}_{1,2}S^{-1} + S^{-T}\tilde{\mathcal{M}}_{1,2}\frac{d}{dt}S^{-1} \end{cases} \tag{10}$$

The full form of $\mathcal{M}^*(g_{12})$ and $\mathcal{C}^*(g_{12}, \zeta^*)$ are presented in Appendix 2. Note that in (10), although the inertia matrix $\mathcal{M}^*$ and its variation $\mathcal{C}^*$ depend on the relative pose g_{12}, their computation is free of mathematical singularities. The use of the SE(3) group to parameterize the relative pose avoids representation problems, e.g., gimbal lock. This proposed formulation is written as follows:

$$\mathcal{M}^*(g_{12})\dot{\zeta}^* + \mathcal{C}^*(g_{12}, \zeta^*)\zeta^* = F^* \tag{11}$$

where $F^* = S^{-\top}\tilde{F}_{1,2} = (F_L,\, F_E,\, \tilde{\tau}_{w_1},\, \tilde{\tau}_{w_2})$,

$$\begin{aligned} \mathcal{M}^*(g_{12}) =& \text{diag}(M_L,\, M_E,\, M_{\theta_1},\, M_{\theta_2}) \\ \mathcal{C}^*(g_{12}, \zeta^*) =& \begin{bmatrix} C_{LL} & C_{LE} & C_{L\theta_1} & C_{L\theta_2} \\ C_{EL} & C_{EE} & C_{E\theta_1} & C_{E\theta_2} \\ -C_{L\theta_1}^T & -C_{E\theta_1}^T & C_{\theta_1} & 0 \\ -C_{L\theta_2}^T & -C_{E\theta_2}^T & 0 & C_{\theta_2} \end{bmatrix}. \end{aligned} \tag{12}$$

Remark 1: Note that (11) preserves the Lagrangian structure (energy) of the total system. This follows because the transformation applied for achieving (11) is passivity-preserving [21]. Also, the two representative systems (locked and shape) are inertia-decoupled [4].

Application to a Hardware-in-the-Loop

The proposed dynamics is suitable to ensure physical consistency of the simulated momentum on a HIL facility for motion simulation, see Fig. 1. In particular, the architecture of the motion replicated on a HIL facility (shape motion) and the simulated mission scenario (locked motion) is illustrated in Fig. 3, where the proposed contribution is emphasized in the dashed box.

The absolute poses of the two modules are computed as,

$$g_i = \int_{t_0}^{t} (g_i V_i^\wedge)\, dt \quad \forall i = 1, 2 \tag{13}$$

where V_i is reconstructed in simulation. This is performed through the relative mapping block in Fig. 3, which computes the initial states by inverting the transformations (2) and (9), as follows

$$(\xi_{in},\, \dot{\theta}_{tot}) = S^{-1}(\xi_{fin}, \dot{\theta}_{tot}) \tag{14}$$

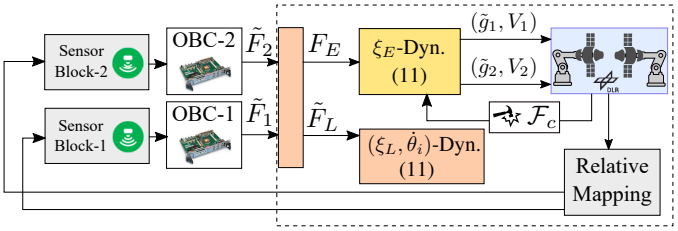

Fig. 3: HIL block diagram with OBC-i actuation mapped as $\tilde{F}_i = (F_i, \tilde{\tau}_{wi})$ to F_E and $\tilde{F}_L = (F_L, \tilde{\tau}_{w1}, \tilde{\tau}_{w2})$, $\mathcal{F}_c$ is the measured interaction wrench between the modules. The industrial robots are commanded using $(\tilde{g}_i, V_i)$. The Relative Mapping block exploits measurements of shape $(\tilde{g}_{12}, V_{12})$ and software-simulated variables $(g_1, \xi_L, \dot{\theta}_1, \dot{\theta}_2)$ to reconstruct all the states.

where $\xi_{in} = (\xi_1, \xi_2)$, $\xi_{fin} = (\xi_L, \xi_E)$, $\dot{\theta}_{tot} = (\dot{\theta}_1, \dot{\theta}_2)$, are the stacked velocities, and therefore, the rigid body velocities of the modules are obtained as,

$$V_i = \xi_i - \begin{bmatrix} 0 \\ \Lambda_i A_i \end{bmatrix} \dot{\theta}_i. \tag{15}$$

The OBC (On-Board Computer) in Fig. 3 represents the controller to be validated on the HIL facility, e.g. for the module 1 (OBC-1) and 2 (OBC-2).

In general, a Cartesian pose or velocity is provided to the position interface of a HIL facility, thus, the robot moves in Cartesian space while exploiting its inverse kinematics, see [22]. For the proposed framework the relative velocity between the commanded motions is then computed as $V_{12} = V_1 - \mathrm{Ad}_{g_{12}}^{-1} V_2$, and the relative pose is computed as,

$$\begin{cases} \tilde{g}_1(t) = \tilde{g}_2(t) g_{12}(t)^{-1}, \\ \tilde{g}_2(t) = g_2(0). \end{cases} \tag{16}$$

This is the final command to the robot, as shown in Fig. 3. In contrast to [16], acceleration measurements and two models per module are not required in the proposed HIL approach.

Note that in (16), the HIL robot $i = 2$ is static, while the robot $i = 1$ simulates the relative motion. In this work, this HIL approach is exploited so that the force sensor that measures the interaction wrench $\mathcal{F}_c$ is attached to the static robot which avoids the sensor's dynamic compensation problem. Thus, $\mathcal{F}_c$ measures the equal and opposing contact forces on the modules. Although one robot is sufficient to simulate relative motions on the HIL, the motion of both modules might be required for validation. In this case, (13) will be integrated to obtain g_i for each module and commanded to each of the HIL robots. This highlights the flexibility of the proposed approach for both HIL implementations.

IV. Proposed Control

The proposed dynamics aids control design for either the locked or relative motion or both simultaneously. If the controller influences only the relative motion, the task is intentionally distributed between the two agents. As a result, one module can uniquely manage the relative pose error. Alternatively, both modules can contribute to the control task with variable weight. This second controller is suitable for the coordinated motion of modules.

In this section, we exploit the dynamics for the two modules, i.e. (11) to propose two novel control laws and prove their stability using Lyapunov's direct method. To that end, the following concepts are introduced from [18, §5.3].

Lemma 1: Considering two poses $\overline{g}(\overline{R}, \overline{p})$, $g(R, p) \in \mathrm{SE}(3)$ for two different frames, the right pose error is given by

$$\eta = \overline{g}^{-1} g = (r,\ R_e),\ r = \overline{R}^T (p - \overline{p}),\ R_e = \overline{R}^T R, \tag{17}$$

Lemma 2: Given two orientations, $\overline{R}, R \in \mathrm{SO}(3)$, an energy function $\phi : \mathrm{SO}(3) \to R_+$ is defined for the potential associated with the orientation difference, as $\phi(R_e) = \frac{1}{2}\mathrm{tr}(K_p(I_3 - R_e))$, and its time-derivative is expressed as $\dot{\phi} = (\mathrm{sk}(K_p R_e)^\vee)^\top \omega$, where ω is the body velocity of R. Here, K_p is the positive proportional gain.

The controller requirements are posed as (g_1, g_{12}) should be regulated about setpoints $(\overline{g}_1, \overline{g}_E)$, which gives the right pose errors $\big((\eta_L(r_L, R_{e_L}), \eta_E(r_E, R_{e_E})\big)$. In contrast to [18, §5.3], which achieved motion tracking of a single rigid body on SE(3), and [3], [4], which achieved formation control of rigid bodies on $\mathrm{SE}(3) \times \mathrm{SE}(3)$, the goal here is to stabilize the motion on $\mathrm{SE}(3) \times (\mathrm{SE}(3) \times \mathbb{R}^3 \times \mathbb{R}^3)$ with coupled dynamics. We achieve this using two controllers in a centralized fashion for a system of multibody modules. The first approach employs both external (RCS) and internal (RWs) actuators simultaneously. The second approach maximizes the RWs usage, thereby reducing fuel consumption and ensuring higher accuracy.[1] Importantly, the RWs response is improved in the control laws by employing the inertia-shaping factors Λ_i^T, which inherently arise through the proposed dynamics in (4). Since we employ a centralized approach, the locked pose error is directly imposed on the $\mathcal{S}_1$. Thus, in the control design, $g_L = g_1$ s.t. $\eta_L = \eta_1$. The controllers are summarized below,

1) Free-flying controller: This controller simultaneously employs the RCS and the RWs toward convergence of the locked and shape regulation tasks (equal priority), while being robust against mutual interactions. This approach is proposed in the theorem below as a passivity-based control law.

Theorem 1: Consider two modules, whose dynamics is modeled in (11), with pose errors $\eta_L(r_L, R_{e_L})$ and $\eta_E(r_E, R_{e_E})$ observed in (17), and velocities $\xi_L(v_L, \mu_L)$, $\xi_E(v_E, \mu_E)$, corresponding to the locked and the shape systems, respectively. Their closed-loop dynamics resulting from the control law, $F^* = (F_L,\ F_E,\ \tilde{\tau}_{w_1},\ \tilde{\tau}_{w_2})$, as

$$F_L = \underbrace{\begin{bmatrix} -\bar{K}_d^L v_L - R_{e_L}^T \bar{K}_p^L r_L \\ -K_d^L \mu_L - \gamma_L \end{bmatrix}}_{\text{feedback}} + \underbrace{F_c^L}_{\text{feedforward}} \tag{18a}$$

$$F_E = \underbrace{\begin{bmatrix} -\bar{K}_d^E v_E - R_{e_E}^T \bar{K}_p^E r_E \\ -K_d^E \mu_E - \gamma_E \end{bmatrix} + A^{*T} \begin{bmatrix} R_{e_L}^T \bar{K}_p^L r_L \\ \gamma_L \end{bmatrix}}_{\text{feedback}} + \underbrace{F_c^E}_{\text{feedforward}} \tag{18b}$$

[1]Under the assumption of continuous-time actuation, both controllers achieve convergence. However, the thruster discretization causes errors, and the second controller outperforms the first in inertial attitude control.

$$\tilde{\tau}_{w_1} = -K_d^1\dot{\theta}_1 - R_{21}^T A_1\gamma_E + A_1\gamma_L + F_c^{w1} \tag{18c}$$
$$\tilde{\tau}_{w_2} = -K_d^2\dot{\theta}_2 + A_2\gamma_E + F_c^{w2} \tag{18d}$$

is uniformly asymptotically stable.

Here, $\gamma_L = \text{sk}(K_p^L R_{e_L})^\vee$, $\gamma_E = \text{sk}(K_p^E R_{e_E})^\vee$ have been used to aid readability and represent the angular potentials, satisfying Lemma 2. The damping gains for translation and angular motions are $D_f = \text{diag}(\bar{K}_d^L, \bar{K}_d^E, K_d^L, K_d^E, K_d^1, K_d^2) \succ 0$, while the proportional gains are $(\bar{K}_p^L, \bar{K}_p^E) \succ 0$ for translation and $(K_p^L, K_p^E) \succ 0$ for the angular motions. The couplings between the representative systems and the RWs are computed using (12) as:

$$\begin{aligned} F_c^L =& C_{L\theta_1}\dot{\theta}_1 + C_{L\theta_2}\dot{\theta}_2,\ F_c^E = C_{E\theta_1}\dot{\theta}_1 + C_{E\theta_2}\dot{\theta}_2 \\ F_c^{w1} =& \Lambda_1 C_{\theta_1 L}\xi_L + \Lambda_1 C_{\theta_1 E}\xi_E + \Lambda_1 C_{\theta_1}\dot{\theta}_1 \\ F_c^{w2} =& \Lambda_2 C_{\theta_2 L}\xi_L + \Lambda_2 C_{\theta_2 E}\xi_E + \Lambda_2 C_{\theta_2}\dot{\theta}_2. \end{aligned}$$

Furthermore, the closed-loop system is output-strict passive, i.e., velocity ζ^* is bounded for bounded disturbances [21].

Before presenting the proof, note that the control law in (18) consists of a PD-type feedback term, and the feedforward term to ensure inertia-shaping.

Proof 1: The stability of the controller is proved through Lyapunov's direct method. The candidate function, W_f, i.e., the total energy of the system, considering a shaping factor $\Lambda_i^\top$ on the RWs inertia, is defined as

$$\begin{aligned} W_f =& \frac{1}{2}\zeta^{*T} M_f \zeta^* + \frac{1}{2}\Delta x_f^T K_f \Delta x_f \\ &+ \frac{1}{2}\text{tr}(K_p^E(I_3 - R_{e_E})) + \frac{1}{2}\text{tr}(K_p^L(I_3 - R_{e_L})) \end{aligned} \tag{19}$$

which satisfies the bounds $\underline{\alpha} \leq W_f \leq \overline{\alpha}$, see Lemma 3 for boundedness argument. Here,

$$\begin{aligned} M_f &= \text{diag}(M_L, M_E, \Lambda_1^T M_{\theta_1}, \Lambda_2^T M_{\theta_2}), \\ \Delta x_f &= (r_L, r_E),\ K_f = \text{diag}(K_p^L, K_p^E). \end{aligned}$$

The derivative of W_f is obtained by exploiting Lemma 2, as

$$\dot{W}_f = \zeta^{*T} M_f \dot{\zeta}^* + \Delta x_f^T K_f \Delta \dot{x}_f + \gamma_E^T \omega_E + \gamma_L^T \omega_1. \tag{20}$$

Reformulating the linear potential and employing (2) and (9), the velocities ω_1 and ω_E are expressed as functions of $\xi_L, \xi_E, \dot{\theta}_1, \dot{\theta}_2$. Thus, the derivative takes the form:

$$\begin{aligned} \dot{W}_f =& \begin{bmatrix} (R_1 K_p^L \Delta x_L)^T & \gamma_L^T \end{bmatrix} \left[\begin{bmatrix} \upsilon_L \\ \mu_L - \Lambda_1 A_1 \dot{\theta}_1 \end{bmatrix} - A^* \begin{bmatrix} \upsilon_E \\ \mu_E \end{bmatrix} \right] \\ &+ \begin{bmatrix} (R_{21}^T K_p^E \Delta x_E)^T & \gamma_E^T \end{bmatrix} \begin{bmatrix} \upsilon_E + p_{21}^\wedge (R_{21}\Lambda_1\dot{\theta}_1) \\ \mu_E + R_{21}\Lambda_1\dot{\theta}_1 - \Lambda_2\dot{\theta}_2 \end{bmatrix} \\ &+ \zeta^{*T} M_f \dot{\zeta}^*. \end{aligned}$$

Introducing the free-flying control law, (18), and leveraging the skew-symmetric property of $\dot{M} - 2C$, we obtain

$$\dot{W}_f = -\zeta^{*T} D_f \dot{\zeta}^* \leq 0. \tag{21}$$

This proves the uniform stability about the equilibrium configurations η_L and η_E. Thus, the system's asymptotic stability is concluded by invoking LaSalle's invariance principle [23]. Next, we prove the robustness against mutual interactions.

Let $F_{d2} = -F_{d1} = \mathcal{F}_c$, be the disturbance on each module (see (1)) due to mutual interaction, resulting in shape and locked disturbance wrenches, $\tilde{F}_E = \mathcal{F}_c$ and $\tilde{F}_L = 0$, respectively, using (11). Considering W_f as the storage function, we get, $\dot{W}_f = -\zeta^{*^\top} D_f \zeta^* + \xi_E^\top \mathcal{F}_c$, which is the proof [21]. □

However, the extensive use of RCS actuation (thruster fuel) imposes limitations on the operation lifespan of the modules. Note that the locked system control requires both modules to be actuated, whereas shape control can be achieved with one.

2) Hierarchical controller: A passivity-based controller, relying on a hierarchy that prioritizes the attenuation of angular momentum of the locked system as a prerequisite before module re-orientation. Thus, each control hierarchy is associated with its corresponding actuator and control law. The first level hierarchical controller utilizes RCS for external actuation and is regulated by the following theorem.

Theorem 2: Consider two modules, whose coupled dynamics is modeled in (11), with linear error functions only, r_L and r_E, observed in (17), and velocities $\xi_L(\upsilon_L, \mu_L)$, $\xi_E(\upsilon_E, \mu_E)$. Their closed-loop dynamics with the first hierarchical control law, $\mathbb{F}_{H1} = (F_L,\ F_E)$, designed as

$$\begin{aligned} F_L =& \underbrace{\begin{bmatrix} -\bar{K}_d^L \upsilon_L - R_{e_L}^T \bar{K}_p^L r_L \\ -K_d^L \mu_L \end{bmatrix}}_{\text{feedback}} + \underbrace{F_c^L}_{\text{feedforward}} \\ F_E =& \underbrace{\begin{bmatrix} -\bar{K}_d^E \upsilon_E - R_{e_E}^T \bar{K}_p^E r_E \\ -K_d^E \mu_E \end{bmatrix} + A^{*T} \begin{bmatrix} R_{e_L}^T \bar{K}_p^L r_L \\ 0 \end{bmatrix}}_{\text{feedback}} \\ &+ \underbrace{F_c^E}_{\text{feedforward}} \end{aligned} \tag{22}$$

is uniformly asymptotically stable.

Here, the couplings, F_c^L and F_c^E, as in Th. 1, are introduced to ensure the inertia-shaping of the RWs. The damping gains are $D_{h_1} = (\bar{K}_d^L, K_d^L, \bar{K}_d^E, K_d^E) \succ 0$, while the proportional gains are $K_{h_1} = (\bar{K}_p^L, \bar{K}_p^E) \succ 0$ for translation.

Proof 2: Consider the Lyapunov candidate function as the sum of the rigid motion kinetic energy and the linear potential energy of the system, as

$$W_{h_1} = \frac{1}{2} V_{h_1}^T M_{h_1} V_{h_1} + \frac{1}{2}\Delta x_{h_1}^T K_{h_1} \Delta x_{h_1} \tag{23}$$

which satisfies the bounds $\underline{\alpha} \leq W_{h_1} \leq \overline{\alpha}$, see Lemma 3 for boundedness argument. Here,

$$M_{h_1} = \text{diag}(M_L, M_E),\ V_{h_1} = (\xi_L, \xi_E),\ \Delta x_{h_1} = (r_L, r_E).$$

The derivative of the candidate is obtained as

$$\dot{W}_{h_1} = V_{h_1}^T M_{h_1} \dot{V}_{h_1} + \Delta x_{h_1}^T K \upsilon_{h_1}. \tag{24}$$

Introducing the first hierarchical control law, (22), and leveraging the skew-symmetric property of $\dot{M} - 2C$, we obtain

$$\dot{W}_{h_1} = -V_{h1}^T D_{h_1} \dot{V}_{h1} \leq 0. \tag{25}$$

This proves the uniform stability of the considered system in the boundaries of the equilibrium positions r_L and r_E, (17),

and of the angular stabilization, i.e. cancellation of momentum that might be gained due to residual errors and inadvertent contacts. The system's asymptotic stability is concluded by invoking LaSalle's invariance principle [23]. □

Consider the set $\Psi = \{\zeta^*, \eta_L, \eta_E | \Delta x_{h1} = 0, V_{h1} = 0\}$ resulting from Th. 2. The second level of the hierarchical controller utilizes internal RWs actuation to achieve reorientation in Ψ as follows.

Theorem 3: Consider two modules with coupled dynamics as modeled in (11), with orientation error functions, R_{e_L} and R_{e_E} from (17), in the set Ψ, which is ensured by Th. 2. The closed-loop dynamics, resulting from the second hierarchical control law, $\mathbb{F}_{H2} = (\tau_{w_1}, \tau_{w_2})$, designed as

$$\begin{cases} \tau_{w_1} = -K_d^1 \dot{\theta}_1 - R_{21}^T \gamma_E + \gamma_L \\ \tau_{w_2} = -K_d^2 \dot{\theta}_2 + \gamma_E \end{cases} \tag{26}$$

with damping gains $D_{h_2} = \text{diag}(K_d^1, K_d^2) \succ 0$ is uniformly asymptotically stable.

Proof 3: Consider the Lyapunov candidate function as the total internal energy of the system, considering a inertia-shaping multiplication factor $\Lambda_i^\top$ on the RWs inertia, as

$$\begin{aligned} W_{h_2} = &\frac{1}{2} \dot{\theta}_{h_2}^T M_{\theta_{h_2}} \dot{\theta}_{h_2} + \frac{1}{2} \text{tr}(K_p^E (I_3 - R_{e_E})) \\ &+ \frac{1}{2} \text{tr}(K_p^L (I_3 - R_{e_L})) \end{aligned} \tag{27}$$

which satisfies the bounds $\underline{\alpha} \leq W_{h_2} \leq \overline{\alpha}$, see Lemma 3 for boundedness argument. Here,

$$M_{\theta_{h_2}} = \text{diag}(\Lambda_1^T M_{\theta_1}, \Lambda_2^T M_{\theta_2}), \ \dot{\theta}_{h_2} = (\dot{\theta}_1, \dot{\theta}_2).$$

The derivative of W_{h_2} is obtained by exploiting Lemma 2, as

$$\begin{aligned} \dot{W}_{h_2} = &\dot{\theta}_{h_2}^T M_{\theta_{h_2}} \ddot{\theta}_{h_2} + \begin{bmatrix} (R_1 K_p^L \Delta x_L)^T & \gamma_L^T \end{bmatrix} \begin{bmatrix} 0 \\ -\Lambda_1 A_1 \dot{\theta}_1 \end{bmatrix} \\ &+ \begin{bmatrix} (R_{21}^T K_p^E \Delta x_E)^T & \gamma_E^T \end{bmatrix} \begin{bmatrix} p_{21}^\wedge (R_{21} \Lambda_1 \dot{\theta}_1) \\ R_{21} \Lambda_1 \dot{\theta}_1 - \Lambda_2 \dot{\theta}_2 \end{bmatrix}. \end{aligned}$$

Introducing the second hierarchical control law, (26), and leveraging the skew-symmetric property of $\dot{M} - 2C$, we obtain

$$\dot{W}_{h_2} = -\dot{\theta}_{h_2}^T D_{h_2} \dot{\theta}_{h_2} \leq 0. \tag{28}$$

This proves the uniform stability of the considered system about the equilibrium orientations R_{e_L} and R_{e_E}, (17). Thus, the system's asymptotic stability is concluded by invoking LaSalle's invariance principle [23]. □

Note that Th. 3 is not independent, and holds in the set Ψ, i.e., Th. 2 is a prerequisite.

V. Validation Results and Discussion

In this section, the two proposed control laws are validated and quantitatively compared using simulation results to emphasize the key differences between them. Additionally, the free-flying controller is experimentally validated on the DLR OOS-SIM using the proposed HIL approach.

The modules are considered to be typical in-orbit demonstration satellites [24] with mass $m = 309\,kg$ and locked inertia $I = \text{diag}(150.2,\ 126.4,\ 126.4)\,kgm^2$, and RWs and RCS

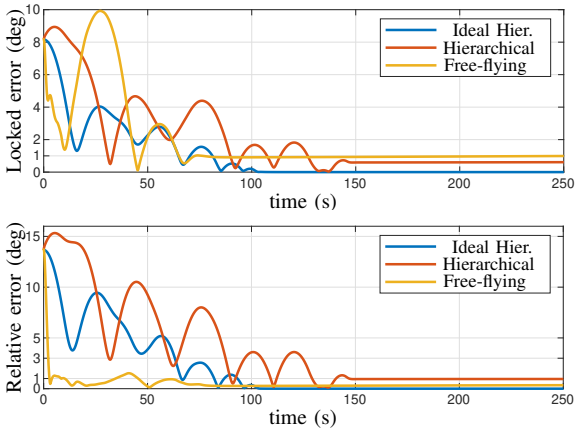

Fig. 4: Comparison of Locked (top) and Relative (bottom) rotational error norms between the hierarchical controller in an ideal scenario with zero initial momentum, and hierarchical and free-flying controllers with non-zero initial momentum.

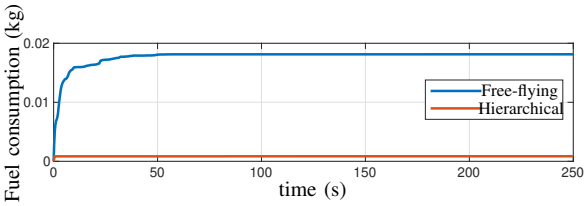

Fig. 5: Comparison between the total average fuel/thruster of the two modules, in the hierarchical and free-flying control modes.

thruster configuration as in [19]. The initial attitude errors are specified as $R_{e_L} \equiv [5.5;\ 4.5;\ 4]^\circ$ and $R_{e_E} \equiv [10;\ 6;\ -6]^\circ$ in the locked and shape systems respectively, while no desired setpoint is set for the translational task. First, an ideal scenario with zero initial angular momentum is simulated. In this case, only the second-level hierarchical controller (Th. 3) is sufficient to ensure convergence of the angular errors, as shown in Fig. 4 (blue). However, in practice, momentum can be non-zero due to factors like discrete RCS actuator dynamics and initial orbital injection. Hence, in the second simulation, an initial momentum is introduced in the simulation as a relative spin of $0.03\ rad/s$ around the y-axis. In this context, the free-flying controller achieves faster orientation convergence by leveraging the full availability of actuators, as shown in Fig. 4 (yellow). Meanwhile, the hierarchical controller (Th. 2 and 3) provides a fuel-efficient solution by limiting RCS usage to the momentum task, as depicted in Fig. 5. This is achieved due to the higher velocity contribution of the RWs in the hierarchical case, as shown in Fig. 6. Furthermore, in Fig. 4 it is observed that a comparable level of accuracy is achieved with the two proposed controllers: the hierarchical controller provides better error behavior in the locked maneuver, while the free-flying controller exhibits lower error in the relative motion. The hierarchical controller is characterized by convergence in a longer time compared to the free-flying controller while ensuring fuel efficiency as its primary advantage. Given that space missions often span extended periods and prioritize fuel conservation, this controller offers a suitable option.

Experimental validation: To experimentally validate the proposed dynamics, (11), the proposed HIL approach in

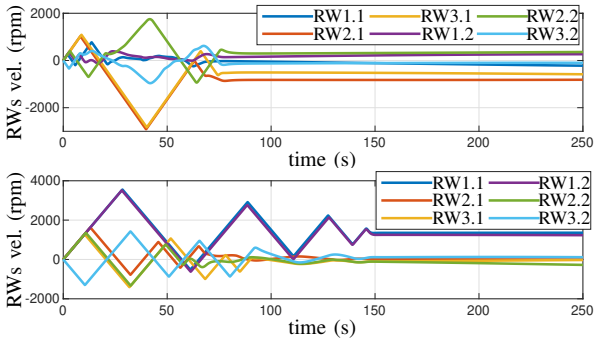

Fig. 6: Contribution of the RWs in terms of velocities in the free-flying (top) and hierarchical (bottom) control modes.

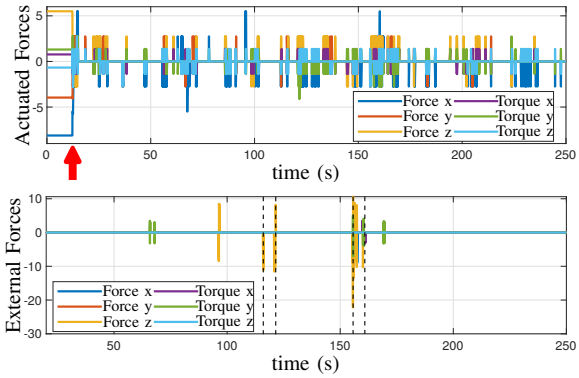

Fig. 7: Leader module's forces actuated by the RCS (top), and contact forces (bottom) over time, obtained from the HIL experiment.

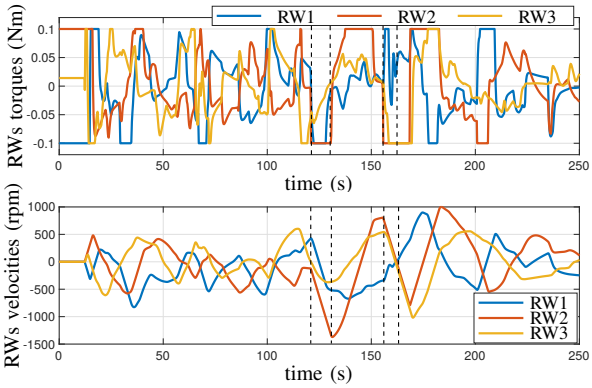

Fig. 8: RWs torques (top), and velocities (bottom) of the leader module over time, obtained from the HIL experiment.

Sec. III was implemented on the DLR OOS-SIM, see Fig. 1. The RWs and RCS were implemented as performance models [19], while the relative rigid motions were replicated using the robotic facility. The simulated mission scenario involved two modules with initial locked momentum around one axis. The leader module was required to perform an approach maneuver towards an unactuated module, which precludes pose control of the locked system as this requires both systems to be actuated. Thus, no setpoint requirements were placed on the locked system. In this setup, the free-flying controller (Th. 1) was required to achieve a desired shape (relative pose) of $[5; 2; 2]\, cm$ and $[2; 2; 0]\,^{\circ}$. The modules are initialized with locked velocity $\xi_L = [0; 0.02; 0]\, rad/s$ and shape velocity $\xi_E = [0.01; 0.02; 0]\, rad/s$.

The free-flying control (Th. 1) was enabled at the time indicated by the arrow at the top of Fig. 7. Mutual interactions were imposed during the HIL experiment by applying a force on the HIL robot ($i = 1$), with peaks at $t = 130\, s$ and $160\, s$, emphasized by dashed lines at the bottom of Fig. 7. These internal forces (measured) appear as interactions between the modules when integrated with the proposed dynamics, (11). Thus, this experiment demonstrates the robustness of the control approach against mutual interactions as explained below. The control task is achieved using RCS forces, Fig. 7, and RWs torques, Fig. 8. The latter are rated for $0.1\, N.m$, as in practical cases [24]. The evolution of relative pose errors is shown in Fig. 9. Here, the relative error only achieves a bounded behaviour as a consequence of the discrete RCS actuation dynamics [19]. Nonetheless, the control strategy remains robust against mutual interactions and the error values stay bounded once the interactions cease. This is relevant for proximity operations, where inadvertent contacts might occur. Fig. 10 shows the key advantage of using the proposed dynamics in the HIL approach: only the shape momentum is affected by the contact disturbances and is regulated by the controller action, while the total momentum dynamics is uncontrolled and is propagated only in software. Note that the HIL simulation was realized without acceleration measurements in contrast to [16]. This experiment validates the proposed free-flying approach to exploit the combined effect of RCS and RWs for motion control of fixed-inertia multibody modules.

VI. Conclusion

In this letter, a momentum-shape formulation of the dynamics is exploited to design, firstly, a novel HIL simulation framework and, secondly, two centralized motion control laws for a fleet of fixed-inertia multibody satellites. The dynamics result from extending the passive decomposition theory, which has previously been limited to rigid bodies. This approach results in dynamics that are inertia-decoupled, singularity-free, and independent of the modules' absolute poses. Both controllers are characterized by inertia-shaping for enhanced responsiveness of RWs, and serve complementary phases (convergence time vs. fuel-efficiency) of the mission to regulate the relative and locked motions of the modules. Furthermore, the free-flying controller is experimentally validated on the DLR OOS-SIM HIL facility. The key advantage of the proposed HIL simulation is that the relative motion is replicated on the hardware while propagating the momentum in the software. This enables the HIL simulation of faster tumbling motions. In future work, the proposed theory will be extended to the n agents case in Fig. 2 and variable inertia systems, e.g., articulated robotic mechanisms.

Appendix

1) Inertia and CC matrices of a single module: The inertia matrix for a single module is observed as $\tilde{\mathcal{M}} = \text{diag}(M, M_\theta)$, where $M = \text{diag}(mI_3, I)$, $M_\theta = A^T I_w (A - \Lambda A)$.

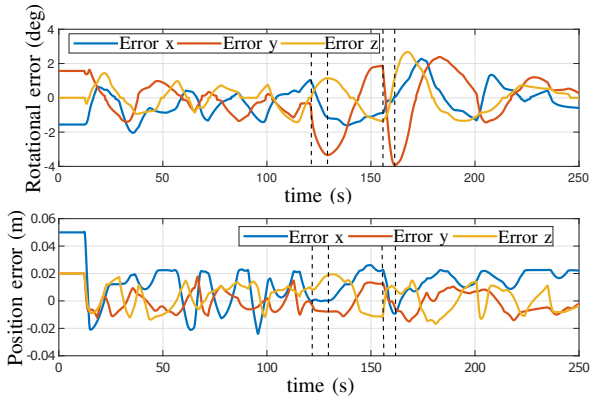

Fig. 9: Relative rotational (top) and translational (bottom) errors over time, obtained from the HIL experiment.

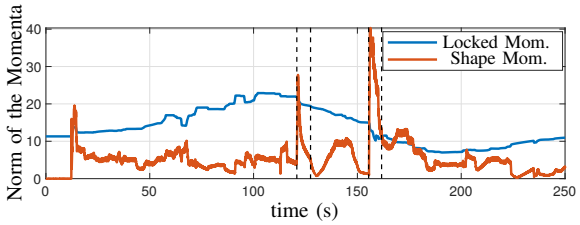

Fig. 10: Norm of the locked (uncontrolled) and shape (controlled) momenta over time, obtained from the HIL experiment.

The CC matrix exhibits a valuable skew-symmetry property among the off-diagonal terms:

$$\tilde{\mathcal{C}} = \begin{bmatrix} \tilde{\mathcal{C}}^{\xi} \\ \tilde{\mathcal{C}}^{\dot{\theta}} \end{bmatrix} = \begin{bmatrix} (\mu - \Lambda A\dot{\theta})^{\wedge} m & 0 & 0 \\ 0 & \mu^{\wedge} I & (I\mu)^{\wedge} \Lambda A \\ 0 & -(A^T \Lambda^T \mu)^{\wedge} I & -(I\mu)^{\wedge} \end{bmatrix}$$

2) Inertia and CC matrices of the proposed dynamics: The overall inertia matrix is expressed as

$$\mathcal{M}^*(g_{12}) = \text{diag}(M_1 + M_2^{(1)}, M_2(I_6 - A^* \text{Ad}_{g_{12}}^{-1}), M_{\theta_1}, M_{\theta_2})$$

The notation $M^{(i)}$ indicates that the inertia matrix is expressed w.r.t the reference frame of module i. A reduced-inertia for the shape system is observed in the second element of R.H.S.

The CC matrix is obtained by recalling the relation $\dot{S}^{-1} = -S^{-1}\dot{S}S^{-1}$ and taking the time derivative of A^* as

$$\begin{aligned} \frac{d}{dt}A^* &= \frac{d}{dt}(M_{tot}^{-1})\text{Ad}_{g_{12}}^{-T} M_2 + M_{tot}^{-1}\frac{d}{dt}(\text{Ad}_{g_{12}}^{-T} M_2) \\ &= -(M_{tot}^{-1}\dot{M}_{tot}M_{tot}^{-1})\text{Ad}_{g_{12}}^{-T} M_2 - M_{tot}^{-1}\text{Ad}_{g_{12}}^{-T}\text{ad}_{v_{12}}^T M_2 \end{aligned}$$

where finally $\dot{M}_{tot} = -\text{Ad}_{g_{12}}^{-T}(\text{ad}_{v_{12}}^T M_2 + M_2 \text{ad}_{v_{12}})\text{Ad}_{g_{12}}^{-1}$.

3) Properties for the stability analysis:

Lemma 3: An energy function, W_f, defined for the multi-body satellite and expressed as the sum of kinetic and potential energies is bounded [25] as $\underline{\alpha} \leq W_f \leq \overline{\alpha}$.

Proof 4: See [25, Lemma 8] for the boundedness property.

REFERENCES

[1] D. Sternberg *et al.*, "Multidisciplinary system design optimization of on orbit satellite assembly architectures," in *IEEE Aerospace Conference*. IEEE, 2015, pp. 1–14.

[2] A. Ruiz *et al.*, "ORU-BOAS: Developing Reusable Building Blocks For Satellite Modularisation," in *74th International Astronautical Congress*, Oct. 2023.

[3] D. Lee and P. Y. Li, "Passive Decomposition Approach to Formation and Maneuver Control of Multiple Rigid Bodies," *Journal of Dynamic Systems Measurement and Control-transactions of The Asme*, vol. 129, pp. 662–677, 2007.

[4] ——, "Passive decomposition of mechanical systems with coordination requirement," *IEEE Transactions on Automatic Control*, vol. 58, no. 1, pp. 230–235, 2012.

[5] M. Okasha, C. Park, and S.-Y. Park, "Guidance and control for satellite in-orbit-self-assembly proximity operations," *Aerospace Science and Technology*, vol. 41, pp. 289–302, 2015.

[6] Q. Hu, Y. Zhang, J. Zhang, and H. Hu, "Formation control of multi-robots for on-orbit assembly of large solar sails," *Acta Astronautica*, vol. 123, pp. 446–454, 2016.

[7] R. Bevilacqua *et al.*, "Guidance navigation and control for autonomous multiple spacecraft assembly: analysis and experimentation," *International Journal of Aerospace Engineering*, vol. 2011, 2011.

[8] R. C. Foust *et al.*, "Autonomous in-orbit satellite assembly from a modular heterogeneous swarm," *Acta Astronautica*, vol. 169, pp. 191–205, 2020.

[9] J. Artigas *et al.*, "The OOS-SIM: An on-ground simulation facility for on-orbit servicing robotic operations," in *Robotics and Automation (ICRA), IEEE International Conference on*, May 2015, pp. 2854–2860.

[10] A. Flores-Abad, O. Ma, K. Pham, and S. Ulrich, "A review of space robotics technologies for on-orbit servicing," *Progress in aerospace sciences*, vol. 68, pp. 1–26, 2014.

[11] T. Boge, T. Wimmer, O. Ma, and T. Tzschichholz, "EPOS - Using Robotics for RvD Simulation of On-Orbit Servicing Missions," *Guidance, Navigation, and Control and Co-located Conferences*, p. 7788, Aug. 2010.

[12] J. Paul *et al.*, "INVERITAS: a facility for hardware-in-the-loop long distance movement simulation for rendezvous and capture of satellites and other autonomous objects," *Acta Astronautica*, vol. 116, pp. 1 – 24, 2015.

[13] A. Pellacani and H. Kolvenbach, "ROSPA, cross-validation of the Platform-ART and ORBIT test facilities for contact dynamic scenario setup and study," in *6th International Conference on Astrodynamics Tools and Techniques, ESA/ESOC*, 2016.

[14] R. Bell, J. Collins, J. Wertz, and L. J. Hansen, "Hardware-in-the Loop Tests of an Autonomous GN&C System for On-orbit Servicing," *AIAA Space 2003 Conference & Exposition*, p. 6372, 2003.

[15] F. Aghili and M. Namvar, "Scaling inertia properties of a manipulator payload for 0-g emulation of spacecraft," *The International Journal of Robotics Research*, 2009.

[16] M. De Stefano, H. Mishra, *et al.*, "A relative dynamics formulation for hardware- in-the-loop simulation of on-orbit robotic missions," *IEEE Robotics and Automation Letters*, vol. 6, no. 2, pp. 3569–3576, 2021.

[17] H. Mishra *et al.*, "Reduced Euler-Lagrange Equations of Floating-Base Robots: Computation, Properties, & Applications," *IEEE Transactions on Robotics*, vol. 39, no. 2, pp. 1439–1457, 2023.

[18] F. Bullo and R. M. Murray, "Tracking for fully actuated mechanical systems: a geometric framework," *Automatica*, vol. 35, no. 1, pp. 17–34, 1999.

[19] A. M. Giordano, A. Dietrich, C. Ott, and A. Albu-Schäffer, "Coordination of thrusters, reaction wheels, and arm in orbital robots," *Robotics and Autonomous Systems*, vol. 131, p. 103564, 2020.

[20] G. Garofalo, B. Henze, J. Englsberger, and C. Ott, "On the inertially decoupled structure of the floating base robot dynamics," *IFAC-PapersOnLine*, vol. 48, no. 1, pp. 322–327, 2015.

[21] R. Ortega, A. Loria, R. Kelly, and L. Praly, "On passivity-based output feedback global stabilization of Euler-Lagrange systems," in *Proceedings of 33rd IEEE Conference on Decision and Control*, vol. 1. IEEE, 1994, pp. 381–386.

[22] M. De Stefano, R. Balachandran, and C. Secchi, "A passivity-based approach for simulating satellite dynamics with robots: Discrete-time integration and time-delay compensation," *IEEE Transactions on Robotics*, vol. 36, no. 1, pp. 189–203, 2020.

[23] J. P. LaSalle, "Stability theory and invariance principles," in *Dynamical systems*. Elsevier, 1976, pp. 211–222.

[24] M. A. Roa *et al.*, "EROSS: In-orbit demonstration of European Robotic Orbital Support Services," in *2024 IEEE Aerospace Conference*, 2024, pp. 1–9.

[25] H. Mishra *et al.*, "A Geometric Controller for Fully-Actuated Robotic Capture of a Tumbling Target," in *American Control Conference (ACC)*, 2020, pp. 2150–2157.